CIRP Journal of Manufacturing Science and Technology 45 (2023) 61–68

Contents lists available at ScienceDirect

CIRP Journal of Manufacturing Science and Technology

journal homepage: www.elsevier.com/locate/cirpj

# Effect of temperature and substrate geometry on single aluminium weld bead geometry deposited by Wire Arc Additive Manufacturing: Proposition of an experimental procedure

Maxime Limousin [a], Supasit Manokruang [a,b], Frédéric Vignat [a,*], Matthieu Museau [a], Christelle Grandvallet [a], Nicolas Béraud [a]

[a] Univ. Grenoble Alpes, CNRS, Grenoble INP, G-SCOP, 38000 Grenoble France
[b] Tools and Die Engineering, Faculty of Engineering, Rajamangala University of Technology Lanna, 128 Huay Kaew Road, Muang, Chiang Mai 50300, Thailand

ARTICLE INFO

*Article history:*
Available online 21 June 2023

*Keywords:*
Wire Arc Additive Manufacturing
Thermal effects
Bead geometry
Experimentation

ABSTRACT

The study of the Wire Arc Additive Manufacturing (WAAM) technology is in expansion mainly thanks to its high deposition rate, its large range of available materials and its inexpensive and wide distribution of its equipment. Being able to control and predict the deposition geometry is a first step toward the technology mastering. To achieve this, numerous studies have focused on the investigation of welding parameters (such as current, tension and energy modulation) and deposition strategies (such as wire feed speed, travel speed, trajectory and dwell time) for a given material. This work proposes to consider two additional parameters, not yet studied, which are the temperature, at which the deposition is made, and the geometry of the substrate receiving the deposition. These two new parameters allow to consider experimental conditions closer to a real fabrication. This study investigates thus their effects on aluminium deposition thanks to an experimental procedure using a heating device and cylindrical substrates of different diameters. Simple simulations are performed to evaluate the thermal conditions of the experiment. From these simulations, a unique indicator is used to represent the whole process conditions. Welded beads are scanned and a circular model is used to model their cross-sections. The implemented experiment shows that the evolution of the dimension of this circle is linked to the evolution of the process conditions. Indeed, hotter conditions, induced either by a higher initial temperature or by different substrate geometries, generate a more spread weld bead. Knowing this trend allows to extract a model and opens the possibility to predict the weld bead dimensions.



## Introduction

For the last few years, the additive manufacturing (AM) technologies have known a huge success and their development has been the topic of numerous research. Not only are they implemented in various sectors (transportation, space, medicine, energy…), they also can have a positive impact on circular economy, re-manufacturing or repurposing [1].

Among AM metallic machines, Direct Energy Deposition has the benefit of producing large structures at a high deposition rate, especially Wire and Arc Additive Manufacturing that offers one of the fastest deposition rates and allows theoretically to shape any type of metal [2–9]. Based on the electric arc welding principle, it is a rather affordable technology that benefits of a machine park well established across all industrial sectors and all over the planet [10]. However, welding stations have been developed precisely for welding assembly but they still lack adjustments for applications in the additive manufacturing field. One of these limitations concerns the production of parts at the intended geometry and many studies strive to understand and reduce geometrical defects in WAAM [11,12]. The management of the deposited geometry is crucial as even a deviation of a tenth in the expected dimensions leads to a mismatch of 1 mm subsequently to ten layers. To be able to achieve large component or near net shape manufacturing, the deposited geometry has to be mastered. This study proposes to enhance our knowledge on this topic by considering the effect of the thermal and geometrical environment of the deposition.

In order to set right the expected deposited geometry, various studies have been committed to link and understand the

* Corresponding author.
*E-mail address:* frederic.vignat@grenoble-inp.fr (F. Vignat).

https://doi.org/10.1016/j.cirpj.2023.06.010
1755-5817/

relationship between various process parameters and the output geometry, the latter usually being defined through the bead height, width and the area of its cross-section [13,14]. Early studies have focused on the role of the input energy (arc voltage U and arc intensity I) and the amount of deposited matter, determined by the Wire Feed Speed (WFS) and the Torch Speed (TS).

Many studies link the evolutions of the weld bead geometry to the variation of the input energy and the amount of deposited matter such as [15–19]. In majority, these process parameters are grouped in a meta-parameter often called "heat input" which actually translates the distribution of the delivered energy per quantity or volume of deposited matter. For part production, other studies have investigated the influence of the chosen torch path strategy either for bead stacking [19–21] or for planar overlapping [22,23]. They bring other parameters or criteria such as the interpass temperature or the dwell time, which introduces in a way the concept of the amount of thermal energy present before the new deposition. These parameters are thus linked to a notion of thermal conditions that highlights the importance of the temperature. However, this aspect remains highly complex as it depends on a large number of parameters such as: the material, input energy, amount of deposited matter, size and geometry of substrate and parts, as well as toolpath strategy. Conditions that define the thermal environment are multifactorial and could present internal interactions.

Different methods are implemented in order to improve the WAAM process or to avoid a drastic thermal evolution such as heat accumulation. One can enumerate cooling systems [24,25], temperature measurements [26] or simulations [27,28], in order to optimize the manufacturing strategy and especially dwell times. However, in these cases, the temperature is not directly controlled and is only known or predicted at the beginning of the weld *i.e.* defined as a starting temperature. If it is accepted that hotter conditions tend to produce different geometries [29], the understanding of the temperature evolution during a fabrication and its impacts on parts geometry is still under-documented. Different approaches exist, some studies try to compile multi-physics model, such as thermal, fluidic, mechanic, metallurgical, electromagnetic [30–32] and [33]. Such complete models still required assumptions to be implemented [33,34], and they demand an important amount of calculation time to be achieved, especially when it comes to large parts. Their efficiency is proven but a more encompassing approach is favoured in this study with a phenomenological approach.

Another factor that is almost not considered in the literature is the substrate evolution and especially its geometry. Conditions have been investigated considering an incline start plate [33] but shape variations of the substrate need to be explored. During a usual additive manufacturing, the considered layer is built on the layer previously deposited. It becomes the new substrate and changes the part geometry as it takes a new shape. Thus, during a fabrication beads are first deposited on flat plates in single track and then in lateral overlap configuration [35], or on wall summit [36] and inside block [37]. For cases with previous depositions, the substrate geometry is almost unknown and its influence on both temperature and bead dimensions on the next deposition is barely considered. In the configuration of a part being manufactured, after the first layer (a), the new bead is deposited either on top of a single bead in case of thin structures (b), or alongside another one in case of overlapping features (b), or on top of such features (d) with possibly another already existing bead on the same layer (e). Those configurations are gathered in Fig. 1 where substrate geometries are highlighted. Even if the second case (b) has been implemented several times, the influence of the substrate geometry on the geometry of the next deposition has been investigated yet in none of these cases.

Thus, in order to achieve the intended part shape after WAAM processing, it is required to control the process parameters. The method proposed in this study is to pilot the initial temperature in order to drive the temperature during the deposition and to establish its relation with the geometrical evolution of the deposited weld bead. The deposition temperature is an aggregate of various influencing factors such as input energy, materials characteristics and many others. It can be obtained thanks to a numerical simulation and can be defined for any part production.

Thus, the aim of this study is to propose a procedure to deposit weld bead under stable and known thermal conditions, faithful to manufacturing conditions, and to link the evolution of the weld bead shape to these conditions.

In order to implement a stable thermal environment, a heating device is used to set up the substrate temperature. Likewise, numerical simulations are used to know precisely the implemented temperature considering welding parameters, substrate geometries *etc*.

In the following sections, this experimental procedure is detailed and applied to aluminium Cold Metal Transfer (CMT) deposition as it has revealed to be a more efficient energy control technology to produce WAAM parts with higher quality [3]. The results are presented and discussed in the last section.

## Experimental procedure

This procedure includes three mains step: beads deposition, thermal numerical simulations and beads geometry measurements.

First of all, single tracks are welded using identical welding parameters. They are deposited on substrates with different curvatures in order to reproduce conditions as close as possible to the reality. To do so, cylinders of different diameters have been used, as their form is closer to a typical weld bead shape as illustrated in Fig. 2. Tests on flat substrates have also been carried out. A heating device has been used in order to establish stable and controlled thermal conditions, with the implementation of a numerical simulation that gives access to the temperature occurring during the process. After their deposition, the constructions have been scanned, bead cross-section have been modelled through a geometrical model and characteristic dimensions have been extracted from it.

The following sections detail each step of this method.

### *Beads deposition*

A production of single beads in different conditions has been run out using a YASKAWA MA1440 Robot and a FRONUIS TPS CMT 4000 Advanced welding station. Beads were deposited in a 5356 aluminium alloy from a 1.2 mm diameter wire. Substrates, regardless of their form and dimensions, are made of a 5083 aluminium alloy. Other parameters that have been kept constant during experiment, such as the energy source regulation, *i.e.* the synergic law, are gathered in Table 1.

In order to change and control conditions in which the deposition is proceeded, two actions have been carried out.

First, the temperature of the substrate before the weld, later called the initial temperature $\boldsymbol{T_{init}}$, is set up thanks to a heating device positioned as illustrated in Fig. 4. A specific attention is given to these conditions: before any deposition, the necessary waiting time is respected in order to ensure that the whole surface, that will receive the new bead, is at the right temperature. It is controlled through temperature measurement thanks to a k-type thermocouple on several positions along the torch path as illustrated Fig. 3. Five different $\boldsymbol{T_{init}}$ have thus been implemented: 25, 100, 200, 300 and 400 °C. These temperatures are chosen to represent different potential manufacturing conditions.

Secondly, modifications of the geometrical environment have been pursued by changing the substrate curvature. Beads were thus welded on different substrates: on flat plates, 250×250×5 $mm^3$, and on cylinders of different diameters (8, 9, 10, 12, 16, 20, 25, 30 and

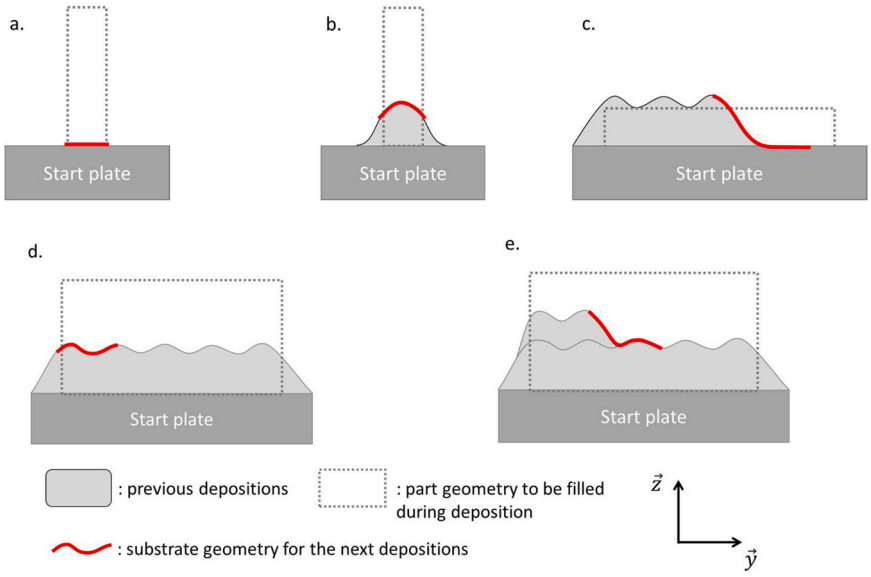


**Fig. 1.** Different substrate geometries encountered during part manufacturing in WAAM.

35 mm). The cylinders are held in place on the flat plates by conducting spot welds at their ends. As previously presented, these different curvatures have been implemented in order to report if a flat substrate produces different bead geometry compared to a curved surface more often encountered during part production. They will also report if these surfaces have an influence on the deposition shape through their degree of curvature. The idea is to observe if beads of different curvatures, as exposed in the Fig. 2.b and relative to different thicknesses, will generate a different geometry for the next deposition.

The use of cylinders will bring another consequence. It has been shown that the location of the deposition in its geometrical environment has an influence on ongoing conditions. In effect, it is well known that, at equivalent welding parameters, the first beads in a wall are deposited in different conditions compared to those in the middle themselves different from those at the wall summit [26]. These differences, linked to the geometrical environment, witness the amount of matter available for thermal energy dissipation and storage in the immediate surrounding of the deposition. In consequence, changing the curvature of the cylinders leads to different size of these substrates and thus, leads to implement different capabilities of the deposition environment to extract and store the thermal energy. After deposition, it appears that for the two smallest diameters (8 and 9 mm), the thermal energy brought to the substrate is enough to partially melt it, gradually deteriorating its originally shape.

**Table 1**
Unchanged parameters.

| | | |
|---|---|---|
| Synergic law | 875 | [-] |
| Wire Feed Speed | 5 | [m.min$^{-1}$] |
| Travel Speed | 0.60 | [m.min$^{-1}$] |
| Gas Flow Rate | 13 | [L.min$^{-1}$] |
| Distance torch/Substrate | 15 | [mm] |
| Travel Angle | 90 | [°] |
| Cross Angle | 90 | [°] |

Across every set of parameters, the useful length of weld beads is equal to 60 mm.

### *Numerical simulation*

As the use of different substrate geometries leads to establish different deposition conditions, a numerical simulation is implemented to clarify these differences, especially in a thermal point of view. To do so, a common criterion is requested to gather all these different conditions under a unique indicator. In order to consider influence of welding parameters, initial temperature and of geometrical environment under a unique data, the indicator $\boldsymbol{T_{dep}}$ is introduced. This indicator is obtained using a numerical simulation, whose parameters are exposed and verified according to [40] and [41]. It is built from the substrate temperature criteria proposed by Chergui and al. [42]. It could be associated to a pyrometer measurement under the Tool Center Point (TCP). Indeed, it corresponds

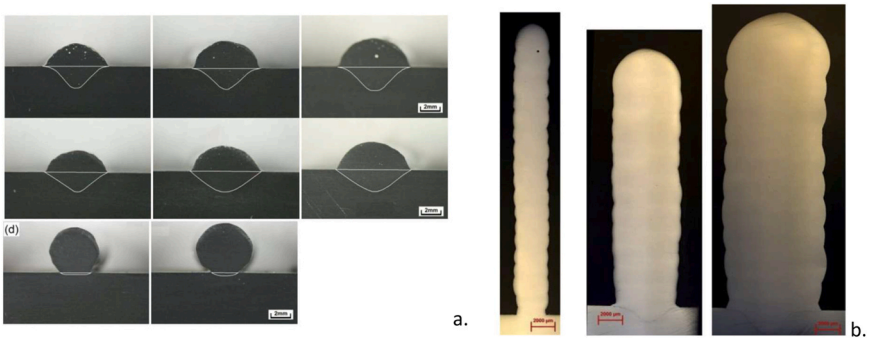


**Fig. 2.** Examples of WAAM production recalling a circular shape for the cross-sections: a. [38],b. [39].

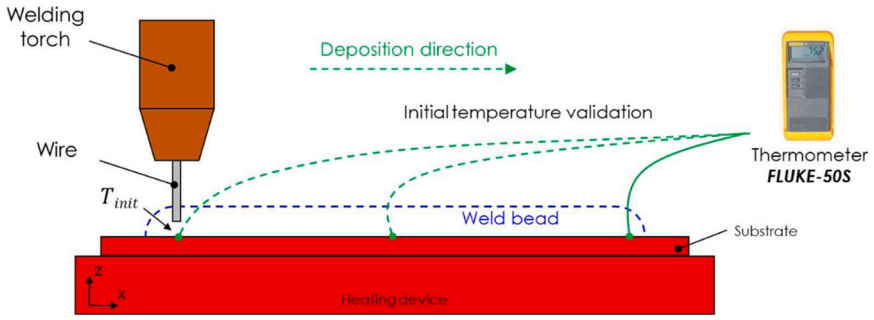


**Fig. 3.** Ante-deposition temperature control.

to the temperature of the substrate portion under the TCP at each time step. It refers to the average temperature of nodes along the bead width and along 1 mm in the deposition direction as illustrated in Fig. 5.

The numerical model has been built considering the geometrical variation of substrates. An example of the evolution of the substrate temperature criterion from Chergui across the deposition is given Fig. 6. For single tracks, a stabilized zone can be identified where the temperature of the substrate is rather constant along the deposition. $\boldsymbol{T_{depStable}}$ is thus defined as the average value of the substrate temperature along this stable zone. The length of this bead portion considered as stable is identical for each configuration and is equal to 60 mm. In this zone, the temperature is stable as far as its variation remains under ± 3.5% around the average value. For the rest of this study, the criteria $\boldsymbol{T_{depStable}}$ is used to account for the process conditions.

The evolution of $\boldsymbol{T_{depStable}}$ is thus obtained, its influences from the initial temperature and from the geometrical environment are illustrated Fig. 7. Most importantly, it shows that $\boldsymbol{T_{depStable}}$ is dependent on the value of $T_{init}$ as expected. It implies that we are able to select a range of value for $\boldsymbol{T_{depStable}}$ according to the initial temperature provided by the thermal device presented in this work.

Secondly, it confirms that the geometrical environment provides an important contribution to deposition conditions during the process. Indeed, for a defined combination of welding parameters and initial temperature, there is a gap of at least 100 °C in the value of $\boldsymbol{T_{depStable}}$ between the smallest and the biggest implemented cylinder. Its contribution to the geometry of the deposited bead is still to be highlighted but it is already possible to say that the influence of the geometrical environment on the process conditions has to be taken into account and characterized.

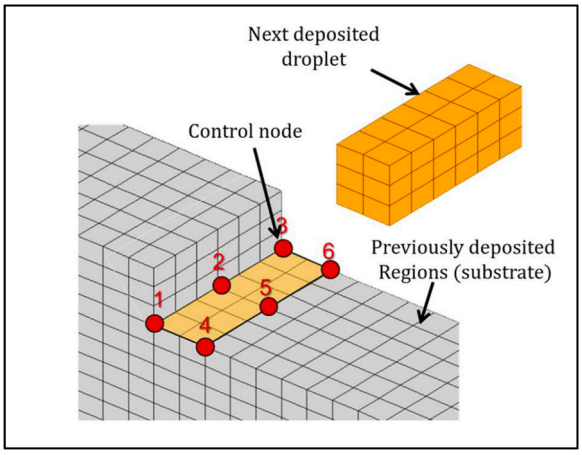


**Fig. 5.** Substrate temperature criterion according to Chergui [42].

*Scan and geometrical bead representation*

As there is no *consensus* on any standardized method for weld bead measurements, and considering that these measurements bring uncertainty, a procedure is proposed and detailed in this study. After fabrication and $\boldsymbol{T_{depStable}}$ evaluation, beads deposited in these different conditions have been scanned with a 3D scanner HandySCAN 700. Numerical representations of the welds are obtained with a resolution of 0.05 mm. From those scans, bead cross-sections are extracted every 1 mm in the stable zone of welds identified in the previous section. Sixty clouds of points are thus obtained for every conditions as illustrated Fig. 8.

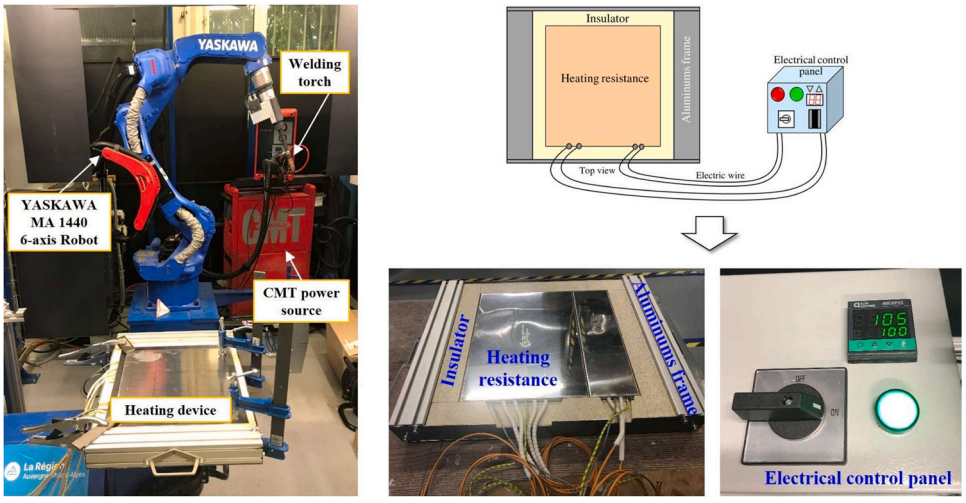


**Fig. 4.** Experimental configuration.

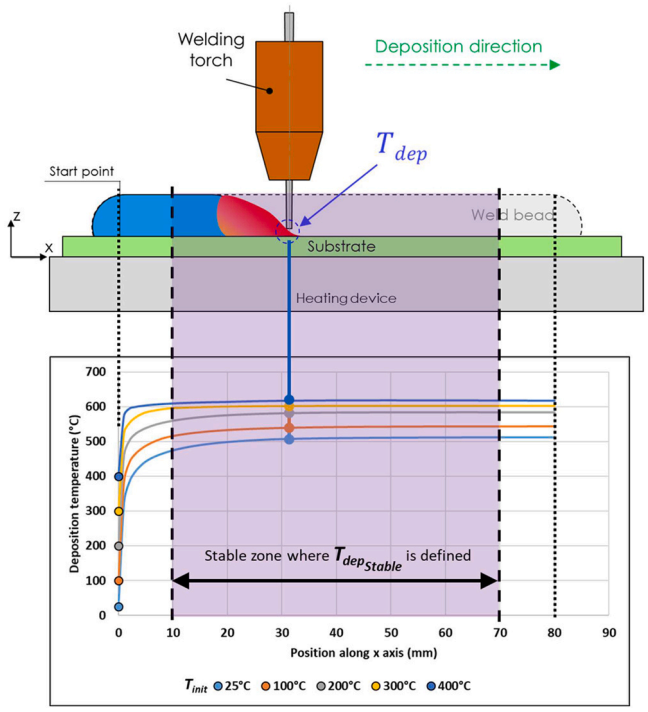


**Fig. 6.** Surface deposition temperature of single tracks deposited on flat substrates under different initial temperature.

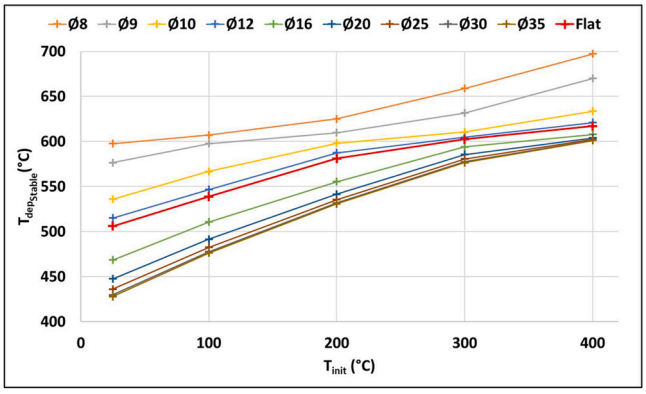


**Fig. 7.** Evolution of $T_{depStable}$ according to the evolution of the initial temperature and of the geometrical environment.

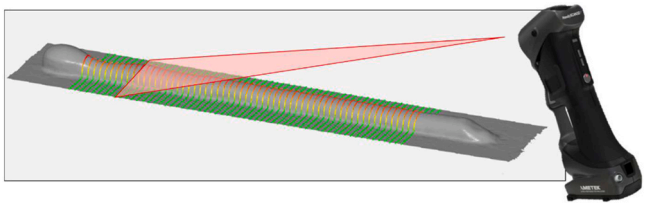

**Fig. 8.** Illustration of the scanning process and extraction of the cross-section profiles.

Although these profiles are a collection of clouds of point, they do not provide characteristic bead dimensions. They must be assigned a geometric model in order to extract representative dimensions. For this purpose, several models exist in the literature for cross-section modelling such as circular arc, parabola, cosine, Gaussian, sine or logistic [43,44]. In this work, the circular model has been chosen since it is the lightest and cylinders represent faithfully the circular shape of beads cross-sections (Fig. 2).

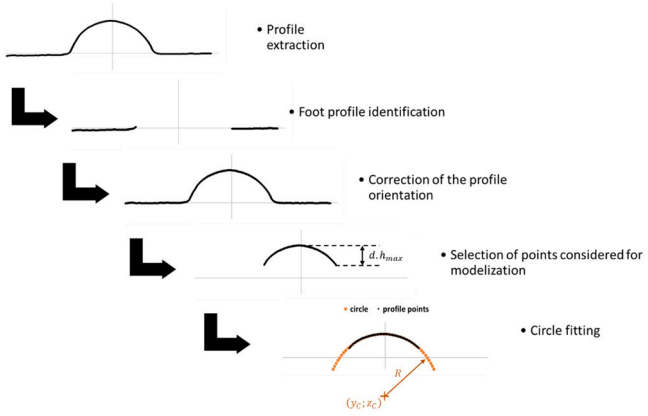


**Fig. 9.** Algorithm of the cloud of point modelling into a circular model.

As detailed in Fig. 9, rough profiles, recorded after scan analysis, are first straightened using profile feet, previously manually selected, in order to ensure that the highest point is correctly identified. Points belonging to the upper surface of beads are then identified from this highest point until a certain distance defined as a ratio **β** of the maximal bead highness. Only these points are used to fit the circular model. A relevant choice of **β** allows reducing results deviations. In effect, too few points induce an irrelevant modelling as a small deviation leads to drastic change in the data model. As illustrated at Fig. 10, form incidents, induced either by the manufacturing or scanning process, may lead to an important error of modelling in case of a too small **β** ratio. These incidents can be limited or avoided with a higher ratio value.

On the other hand, a too high value of **β** may include points belonging to the bead foot that can be subject to errors during the scanning process due to access issue.

The circle model is fitted thanks to the least square method on these selected points. The main outputs of the algorithm are the radius of the circle, the coordinates of its center and the residue obtained according to Eq. (1).

$$residue = \frac{\sum (distance_{point\ \ to\ \ circle\ \ center} - radius)^2}{number\ \ of\ \ considered\ \ points} \quad (1)$$

In order to insure that this geometrical model and its implementation are able to represent correctly the bead cross-section, several dimensional criteria have to be verified. They include the area of the cross-section, as it witnesses the real amount of deposited matter, and both the maximal profile highness $\boldsymbol{h_{max}}$ and the width at mid-height $\boldsymbol{w_{h_{max}/2}}$ which are dimensions used in the trajectory definition such layer increment or lateral bead overlap. All of these criteria are both extracted from profiles, as defined in Fig. 11, and calculated from the circular model for the flat plates experiment. The comparison of the control dimensions $k_i$ values (the maximal highness, the width at mid-height and the area under the curve) will be also used to determine the most efficient value of the **β** parameter among 20%, 40%, 60% and 80% as specified in Eq. (2).

$$\Delta k_i = k_i^{profile} - k_i^{circle} \quad (2)$$

The results of this comparison are gathered at Fig. 12. They highlight that a value of 60% for the **β** parameter seems to be a good compromise and lead to a model very close to the scanned profiles: a deviation of few hundredths for $\boldsymbol{h_{max}}$, a few tenths for $\boldsymbol{w_{h_{max}/2}}$ and a few percentages of difference in the ***area*** of the cross-section. This value of 60% is chosen for compromise. Lower values are less precise to represent the amount of deposited matter (the ***area***) or the width at mid-height. The last value of 80% was not chosen because it slightly loses accuracy to represent $\boldsymbol{h_{max}}$ while the bead cross-section ***area*** and $\boldsymbol{w_{h_{max}/2}}$ are equivalent.

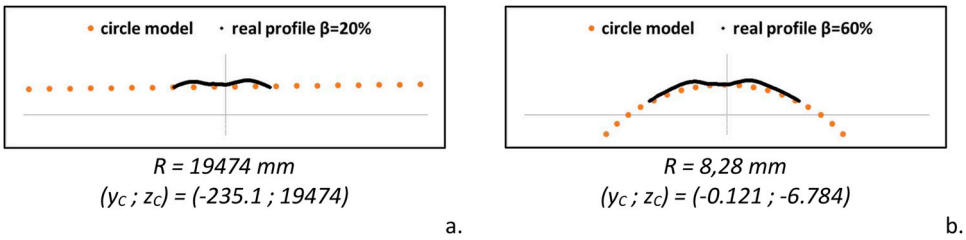


**Fig. 10.** Illustration of an irrelevant (a) and relevant (b) choice of the **β** parameter with a profile of the experiment at 400 °C on a flat plate.

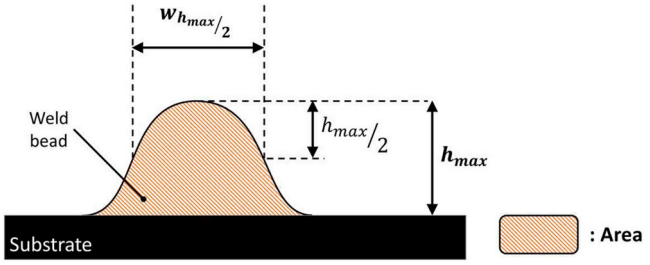


**Fig. 11.** Definition of control dimensions.

The **β** parameter is therefore fixed at a value of 60% for the rest of this work. It also allows to validate the accuracy of the algorithm, which makes it possible to account for a sufficient precision for tracking potential evolutions due to changes of the process conditions.

## Results and discussion

As the criterion $\boldsymbol{T_{depStable}}$ is able to translate both thermal and geometrical condition at an appropriate level, it is used as unique indicator to transcribe the process conditions. This choice of representation seems relevant and is in accordance with the observation of the bead radius evolution according to $\boldsymbol{T_{depStable}}$. Highlighted in Fig. 13, every conditions of different initial temperatures or of different substrates gather in a single trend where a hotter $\boldsymbol{T_{depStable}}$ leads to larger value of the bead radius. Hotter thermal conditions induce a larger bead radius as both the viscosity and the surface tension of a hotter liquid metal are lowered, leading to an easier spread of the metal. Furthermore, this behaviour does not depend on the substrate geometry apart from its contribution on

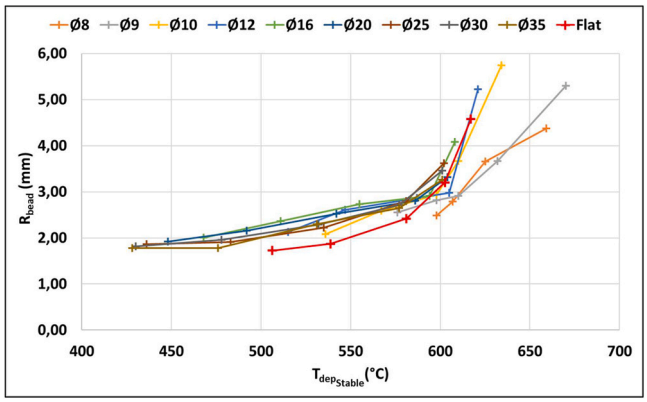


**Fig. 13.** Evolution of the bead radius considering $\boldsymbol{T_{depStable}}$.

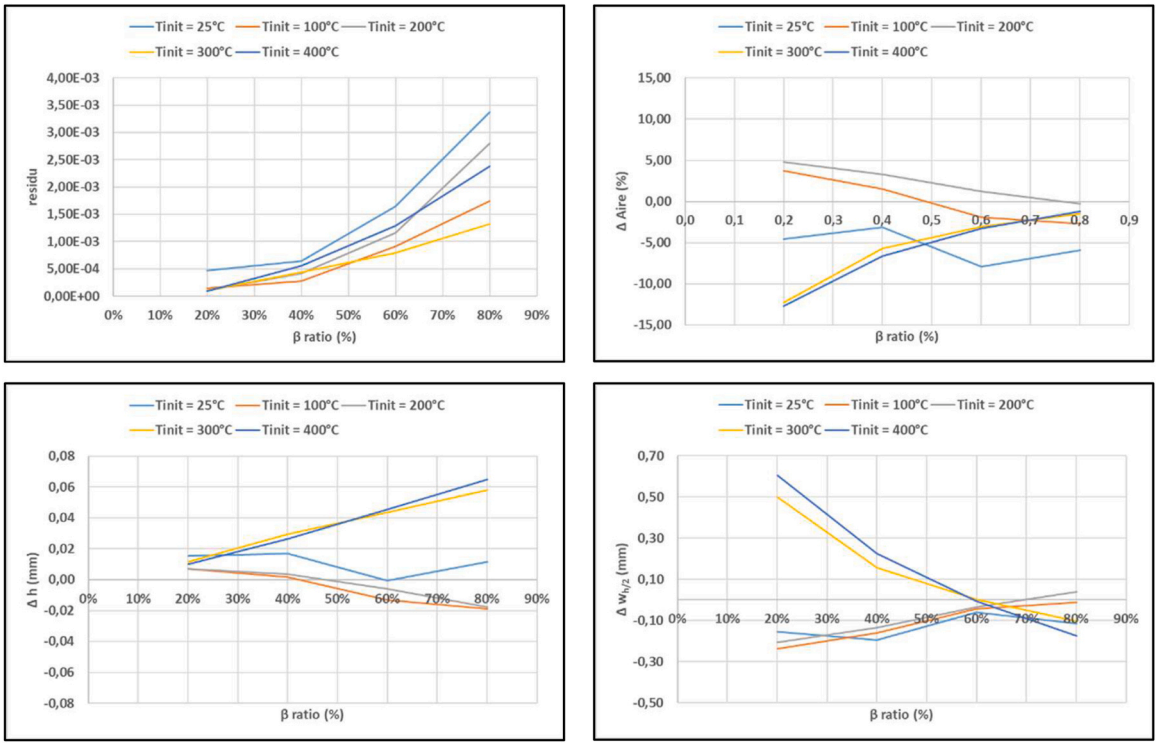


**Fig. 12.** Deviation between direct scan reading and circular model extraction.

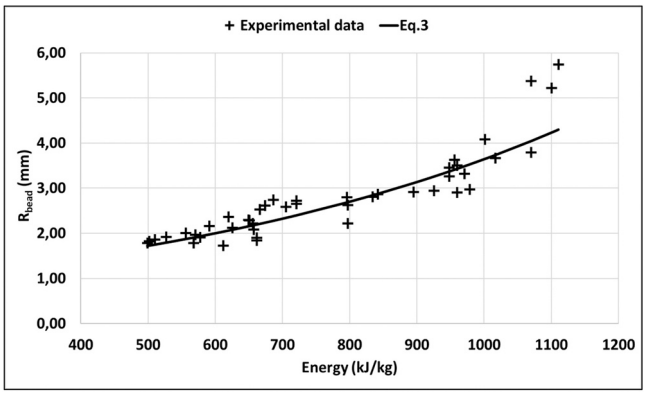


**Fig. 14.** Evolution of the bead radius considering $E_{thermal}$.

the thermal condition previously shown. As the total amount of deposited matter should not change, the width and height of the bead should evolve in consequence. It implies that knowing the thermal criterion is enough to predict these geometrical dimensions.

For such prediction, a model is proposed in Fig. 14. It is built from the presented data set and by transposing $T_{depStable}$ into thermal energy per unit of matter, further called $E_{thermal}$ [kJ/kg]. Data for cylinders of 8 and 9 mm diameter are not considered as these conditions have induced a too important deterioration of substrates. Values for heat capacity and enthalpy of fusion are gathered from [41]. It is then possible to link the evolution of the radius of bead cross-sections to this thermal energy associated to $T_{depStable}$ using the formula expressed in Eq. 3. The correlation coefficient reaches about 0858.

$$R_{bead} = 0,8124.\ e^{0,0015.E_{thermal}} \quad (3)$$

## Conclusion

The aim of this study is to propose a procedure to deposit weld bead under stable and known thermal conditions, and to link the evolution of the weld bead shape to these conditions. It has been shown that the literature currently misses the consideration of both the thermal and geometrical environment in which the deposition is processed. This research work focused on implementing an experimental procedure to explore their influence on the bead geometry.

To do so, a heating device has been used to set up a desired initial temperature. Bead deposition has been then processed on a selection of different substrate curvatures thanks to cylinders of various diameters settled as substrates.

Numerical simulations have been computed to understand more deeply these conditions. They highlight a stable zone along the deposition where the temperature is considered as constant. From it, a unique indicator $T_{depStable}$ is extracted and used to represent these conditions.

Beads have been scanned after deposition. It has been shown that a portion of a circle can represent the cross-section of beads. Verifications have been pursued and a precision of few hundredths can be achieved to obtain the bead dimensions from this circular model.

Finally, the experiment highlights that the circle radius associated to the bead cross-section increases according to the rise of $T_{depStable}$. A model is proposed to link this dimension to the process conditions over the considered temperature range.

To conclude, the procedure exposed in this study allows to reproduce different thermal conditions which stability has been demonstrated through simulation and bead scanning. The variation of these conditions highlights the link between the weld bead geometry, the thermal conditions and the substrate geometry. The aggregation of the different factors influencing the temperature under a unique criterion $T_{depStable}$ is a key result of this study.

As perspectives, this work can be completed by considering various welding parameters such as tension, intensity, wire feed speed or travel speed, and by investigating different materials in order to enhance the predictive model. These equations describing the evolution of bead dimensions could also be used in realistic simulation to predict beads and part shapes produced by WAAM. They could ultimately be used to feed Computer Aided Manufacturing (CAM) software and help establishing toolpath trajectory or choosing optimised process parameters.

## Declaration of Competing Interest

The authors declare that they have no known competing financial interests or personal relationships that could have appeared to influence the work reported in this paper.

## Acknowledgement

Funding acknowledgement have to be awarded to the Ministry of Higher Education, Science, Research and Innovation, Thai government.

## References

[1] Kandukuri, S., Günay, E.E., Al-Araidah, O., Okudan Kremer, G.E., 2021, Inventive Solutions for Remanufacturing Using Additive Manufacturing: ETRIZ. Journal of Cleaner Production, vol. 305:126992. https://doi.org/10.1016/j.jclepro.2021.126992.
[2] Wu, B., et al., 2018, A Review of the Wire Arc Additive Manufacturing of Metals: Properties, Defects and Quality Improvement. Journal of Manufacturing Processes, vol. 35:127–139. https://doi.org/10.1016/j.jmapro.2018.08.001.
[3] Raut, L.P., Taiwade, R.V., 2021, Wire Arc Additive Manufacturing: A Comprehensive Review and Research Directions. Journal of Materials Engineering and Performance, vol. 30/7: 4768–4791. https://doi.org/10.1007/s11665-021-05871-5.
[4] Cooke, S., Ahmadi, K., Willerth, S., Herring, R., 2020, Metal Additive Manufacturing: Technology, Metallurgy and Modelling. Journal of Manufacturing Processes, vol. 57:978–1003. https://doi.org/10.1016/j.jmapro.2020.07.025.
[5] Çam, G., 2022, Prospects of Producing Aluminum Parts by Wire Arc Additive Manufacturing (WAAM). Materials Today: Proceedings, vol. 62:77–85. https://doi.org/10.1016/j.matpr.2022.02.137.
[6] Xiong, Y., Tang, Y., Zhou, Q., Ma, Y., Rosen, D.W., 2022, Intelligent Additive Manufacturing and Design: State of the Art and Future Perspectives. Additive Manufacturing, vol. 59:103139. https://doi.org/10.1016/j.addma.2022.103139.
[7] Günen, A., Gürol, U., Koçak, M., Çam, G., 2023, A New Approach to Improve Some Properties of Wire Arc Additively Manufactured Stainless Steel Components: Simultaneous Homogenization and Boriding. Surface and Coatings Technology, vol. 460:129395. https://doi.org/10.1016/j.surfcoat.2023.129395.
[8] Günen, A., Gürol, U., Koçak, M., Çam, G., 2023, Investigation into the Influence of Boronizing on the Wear Behavior of Additively Manufactured Inconel 625 Alloy at Elevated Temperature. Progress in Additive Manufacturing. https://doi.org/10.1007/s40964-023-00398-8.
[9] Ceritbinmez, F., Günen, A., Gürol, U., Çam, G., 2023, A Comparative Study on Drillability of Inconel 625 Alloy Fabricated by Wire Arc Additive Manufacturing. Journal of Manufacturing Processes, vol. 89:150–169. https://doi.org/10.1016/j.jmapro.2023.01.072.
[10] Verified Market Research, 'Global Welding Equipment Market'. 2022.
[11] Laghi, V., Palermo, M., Gasparini, G., Alena Girelli, V., Trombetti, T., 2019, Geometrical Characterization of Wire-and-Arc Additive Manufactured Steel Element. Advanced Materials Letters, vol. 10/10: 695–699. https://doi.org/10.5185/amlett.2019.0019.
[12] Chen, X., et al., 2021, A Review on Wire-arc Additive Manufacturing: Typical Defects, Detection Approaches, and Multisensor Data Fusion-based model. The International Journal of Advanced Manufacturing Technology, vol. 117/3–4: 707–727. https://doi.org/10.1007/s00170-021-07807-8.
[13] Pinto-Lopera, J., Motta, J.S.T., Absi Alfaro, S., 2016, Real-Time Measurement of Width and Height of Weld Beads in GMAW Processes. Sensors, vol. 16/9: 1500. https://doi.org/10.3390/s16091500.
[14] Zhao, Y., Li, W., Liu, A., 2020, Optimization of geometry quality model for wire and arc additive manufacture based on adaptive multi-objective grey wolf algorithm. Soft Computing, vol. 24/22: 17401–17416. https://doi.org/10.1007/s00500-020-05027-y.
[15] Aloraier, A., Almazrouee, A., Shehata, T., Price, J.W.H., 2012, Role of Welding Parameters Using the Flux Cored Arc Welding Process of Low Alloy Steels on

Bead Geometry and Mechanical Properties. Journal of Materials Engineering and Performance, vol. 21/4: 540–547. https://doi.org/10.1007/s11665-011-9948-6.
[16] Suryakumar, S., Karunakaran, K.P., Bernard, A., Chandrasekhar, U., Raghavender, N., Sharma, D., 2011, Weld Bead Modeling and Process Optimization in Hybrid Layered Manufacturing. Compututer -Aided Design, vol. 43/4: 331–344. https://doi.org/10.1016/j.cad.2011.01.006.
[17] Cong, B., Ouyang, R., Qi, B., Ding, J., 2016, Influence of Cold Metal Transfer Process and Its Heat Input on Weld Bead Geometry and Porosity of Aluminum-Copper Alloy Welds. Rare Metal Materials and Engineering, vol. 45/3: 606–611. https://doi.org/10.1016/S1875-5372(16)30080-7.
[18] Ma, B., Zhang, N., Zhang, Y., Gao, X., 2021, Welding Parameters Effect And Optimization on Bead Geometry During Arc Additive Manufacturing. Journal of Physics: Conference Series, vol. 1986/1:012034. https://doi.org/10.1088/1742-6596/1986/1/012034.
[19] Yildiz, A.S., Davut, K., Koc, B., Yilmaz, O., 2020, Wire arc additive manufacturing of High-strength Low Alloy Steels: Study of Process Parameters and Their Influence on the Bead Geometry and Mechanical Characteristics. Int J Adv Manuf Technol, vol. 108/11–12: 3391–3404. https://doi.org/10.1007/s00170-020-05482-9.
[20] Ding, D.-H., Pan, Z.-X., Dominic, C., Li, H.-J., 2015, 'Process Planning Strategy for Wire and Arc Additive Manufacturing', in *Robotic Welding, Intelligence and Automation*. Tarn T-J, Chen S-B, Chen X-Q, (Eds.) Advances in Intelligent Systems and Computing,, vol. 363. Cham: Springer International Publishing: 437–450. https://doi.org/10.1007/978-3-319-18997-0_37.
[21] Ayarkwa, K.F., Williams, S., Ding, J., 2015, Investigation of pulse advance cold metal transfer on aluminium wire arc additive manufacturing. International Journal of Rapid Manufacturing, vol. 5/1: 44. https://doi.org/10.1504/IJRAPIDM.2015.073547.
[22] Wang, X., Wang, A., Li, Y., 2019, A Sequential Path-planning Methodology for Wire and Arc Additive Manufacturing Based on a Water-pouring Rule. The International Journal of Advanced Manufacturing Technology, vol. 103/9–12: 3813–3830. https://doi.org/10.1007/s00170-019-03706-1.
[23] Ferreira, R.P., Scotti, A., 2021, The Concept of a Novel Path Planning Strategy for Wire + Arc Additive Manufacturing of Bulky Parts: Pixel. Metals, vol. 11/3: 498. https://doi.org/10.3390/met11030498.
[24] Montevecchi, F., Venturini, G., Grossi, N., Scippa, A., Campatelli, G., 2018, Heat Accumulation Prevention in Wire-Arc-Additive-Manufacturing Using Air Jet Impingement. Manufacturing Letters, vol. 17:14–18. https://doi.org/10.1016/j.mfglet.2018.06.004.
[25] Reisgen, U., Sharma, R., Mann, S., Oster, L., 2020, Increasing the Manufacturing Efficiency of WAAM by Advanced Cooling Strategies. Weld World, vol. 64/8: 1409–1416. https://doi.org/10.1007/s40194-020-00930-2.
[26] Kozamernik, N., Bračun, D., Klobčar, D., 2020, WAAM System with Interpass Temperature Control and Forced Cooling for Near-net-shape Printing of Small Metal Components. The International Journal of Advanced Manufacturing Technology, vol. 110/7–8: 1955–1968. https://doi.org/10.1007/s00170-020-05958-8.
[27] Geng, H., Li, J., Xiong, J., Lin, X., 2017, Optimisation of Interpass Temperature and Heat Input for Wire and Arc Additive Manufacturing 5A06 Aluminium Alloy. Science and Technology of Welding and Joining, vol. 22/6: 472–483. https://doi.org/10.1080/13621718.2016.1259031.
[28] Montevecchi, F., Venturini, G., Grossi, N., Scippa, A., Campatelli, G., 2018, Idle Time Selection for Wire-arc Additive Manufacturing: A Finite Element-based Technique. Additive Manufacturing, vol. 21:479–486. https://doi.org/10.1016/j.addma.2018.01.007.
[29] Robert, P., Museau, M., Paris, H., 2018, Effect of Temperature on the Quality of Welding Beads Deposited with CMT Technology. 2018 IEEE International Conference on Industrial Engineering and Engineering Management (IEEM). IEEE,, Bangkok: 680–684. https://doi.org/10.1109/IEEM.2018.8607636.
[30] Ogino, Y., Asai, S., Hirata, Y., 2018, Numerical simulation of WAAM process by a GMAW weld pool model. Weld World, vol. 62/2: 393–401. https://doi.org/10.1007/s40194-018-0556-z.
[31] Cadiou, S., Courtois, M., Carin, M., Berckmans, W., Le masson, P., 2020, 3D heat transfer, fluid flow and electromagnetic model for cold metal transfer wire arc additive manufacturing (Cmt-Waam). Additive Manufaturing. https://doi.org/10.1016/j.addma.2020.101541.
[32] Hu, Z., Hua, L., Qin, X., Ni, M., Ji, F., Wu, M., 2021, Molten Pool Behaviors and Forming Appearance of Robotic GMAW on Complex Surface With Various Welding Positions. Journal of Manufacturing Processes, vol. 64:1359–1376. https://doi.org/10.1016/j.jmapro.2021.02.061.
[33] Cao, H., Huang, R., Yi, H., Liu, M., Jia, L., 2022, Asymmetric Molten Pool Morphology in Wire-arc Directed Energy Deposition: Evolution Mechanism and Suppression Strategy. Additive Manufacturing, vol. 59:103113. https://doi.org/10.1016/j.addma.2022.103113.
[34] Mohebbi, M.S., Kühl, M., Ploshikhin, V., 2020, A Thermo-capillary-gravity Model for Geometrical Analysis of Single-bead Wire and Arc Additive Manufacturing (WAAM). The International Journal of Advanced Manufacturing Technology, vol. 109/3–4: 877–891. https://doi.org/10.1007/s00170-020-05647-6.
[35] Li, Y., Sun, Y., Han, Q., Zhang, G., Horváth, I., 2018, Enhanced Beads Overlapping Model for Wire and Arc Additive Manufacturing of Multi-layer Multi-bead Metallic Parts. Journal of Materials Processing Technology, vol. 252:838–848. https://doi.org/10.1016/j.jmatprotec.2017.10.017.
[36] Prado-Cerqueira, J., et al., 2018, Analysis of Favorable Process Conditions for the Manufacturing of Thin-Wall Pieces of Mild Steel Obtained by Wire and Arc Additive Manufacturing (WAAM). Materials, vol. 11/8: 1449. https://doi.org/10.3390/ma11081449.
[37] Cong, B., Qi, Z., Qi, B., Sun, H., Zhao, G., Ding, J., 2017, A Comparative Study of Additively Manufactured Thin Wall and Block Structure with Al-6.3%Cu Alloy Using Cold Metal Transfer Process. Apples Science, vol. 7/3: 275. https://doi.org/10.3390/app7030275.
[38] Cong, B., Ding, J., Williams, S., 2015, Effect of Arc Mode in Cold Metal Transfer Process on Porosity of Additively Manufactured Al-6.3%Cu Alloy. The International Journal of Advanced Manufacturing Technology, vol. 76/9–12: 1593–1606. https://doi.org/10.1007/s00170-014-6346-x.
[39] Ali, Y., Henckell, P., Hildebrand, J., Reimann, J., Bergmann, J.P., Barnikol-Oettler, S., 2019, Wire Arc Additive Manufacturing of Hot Work Tool Steel With CMT Process. Journal of Materials Processing Technology, vol. 269:109–116. https://doi.org/10.1016/j.jmatprotec.2019.01.034.
[40] Chergui, A., Villeneuve, F., Béraud, N., Vignat, F., 2022, Thermal Simulation of Wire Arc Additive Manufacturing: A New Material Deposition and Heat Input Modelling. The International Journal on Interactive Design and Manufacturing (IJIDeM), vol. 16/1: 227–237. https://doi.org/10.1007/s12008-021-00824-7.
[41] Béraud, N., Chergui, A., Limousin, M., Villeneuve, F., Vignat, F., 2022, An indicator of porosity through simulation of melt pool volume in aluminum wire arc additive manufacturing. Mech India, vol. 23:1. https://doi.org/10.1051/meca/2021052.
[42] Chergui, M.A., 2021, Simulation Based deposition Strategies Evaluation and Optimization in Wire Arc Additive Manufacturing. Université Grenoble Alpes.
[43] Cao, Y., Zhu, S., Liang, X., Wang, W., 2011, Overlapping Model of Beads and Curve Fitting of Bead Section for Rapid Manufacturing by Robotic MAG Welding Process. Robotics and Computer-Integrated Manufacturing, vol. 27/3: 641–645. https://doi.org/10.1016/j.rcim.2010.11.002.
[44] Ding, D., Pan, Z., Cuiuri, D., Li, H., 2015, A Multi-bead Overlapping Model for Robotic Wire and Arc Additive Manufacturing (WAAM). Robotics and Computer-Integrated Manufacturing, vol. 31:101–110. https://doi.org/10.1016/j.rcim.2014.08.008.